THE JOURNAL OF THE ACOUSTICAL SOCIETY OF KOREA Vol.29, No.2E 2010. 6. pp. 73-85

High Frequency Ultrasound and Its Applications to Animal and Human Imaging Focusing on Vessel and Blood

Tae-Hoon Bok*, Dong-Guk Paeng*
*Department of Ocean System Engineering, College of Ocean Science, Jeju National University
(Received June 9, 2010; accepted June 28, 2010)

Abstract

In the diagnostic ultrasound (US) transducer technology, the high frequency US (HFUS) transducer over 20 MHz is one of the current issues to be pursued for better resolution with the expense of penetration. HFUS single element transducers and the mechanical scanning systems for imaging are reviewed, and HFUS array transducers are also briefly summarized. HFUS applications such as the human applications in ophthalmology and dermatology and small animal applications for research purposes are reviewed with vascular and blood imaging in this paper.

Keywords: *High frequency ultrasound, transducer array, ultrasonic imaging, blood vessel*

I. Introduction

In the diagnostic ultrasound (US) technology, there are two research directions for researchers to pursue currently. One is to develop 2 dimensional (D) array transducers for real time 3D imaging, which would be useful to diagnose the diseases related with the dynamical cardiac motion and blood vessels. The other is to develop high frequency US (HFUS) transducers over 20 MHz for better resolution. With the expense of penetration depth, the spatial resolution would go up to 15 μm for 100 MHz. There are two spatial resolutions, namely axial resolution and lateral resolution. Axial resolution is the resolution along the beam propagation, and proportional to pulse duration and defined by one of bandwidth. Lateral resolution is the resolution along the perpendicular direction of the beam propagation, and defined to f-number multiplied by a wavelength, where f-number is focal length divided by the diameter of a transducer. Axial resolution is improved as freguency in creases, reaching up to 10 μm for 150 MHz, and lateral resolution reaching up to 10 μm for f-number of 0.7. However, due to increase of attenuation coefficient in tissue with frequency, the penetration depth is limited to a few millimeters for 100 MHz and higher frequencies. Therefore, the applications of HFUS are limited due to the smaller penetration depth.

The most active applications of HFUS are in small animal experiments for research purposes. Mouse, rat, and zebra fish are the main species for HFUS applications. In human applications, ophthalmology and dermatology are the two main application areas. Skin tissue is relatively high attenuated but the

Corresponding author: Dong-Guk Paeng (paeng@jejunu.ac.kr)
Department of Oceanic Information and System Engineering, College of Ocean Science, Jeju National University, 66 Jejudae-hakno, Jeju-si, Jeju Special Self-Governing Province

penetration depth for diagnosis is required to be small, so the dermatological applications of HFUS are explored and investigated. The attenuation of anterior part of the eye tissue except lens is small so that HFUS is appropriate for imaging of the anterior part of the eye. Currently, this anterior imaging of the eye is the most popular human application of HFUS and several commercialized HFUS systems are currently available. Recently the posterior section including retinal vessels was also investigated with minimally invasive HFUS needle transducers. Another HFUS application has been suggested in blood imaging, which could investigate the dynamical change of red blood cell (RBC) aggregation in blood *in situ* noninvasively. The summary of the near-future direction of transducer technology is shown in Fig. 1.

It is hard to develop array transducers and the corresponding electronic systems with image processing for HFUS. Recently Foster et al (2009) have developed commercialized HFUS array transducers and the electronic system, which was released by Visualsonics Ltd. in 2008 for the first time in the world [1]. Another research group independently developed HFUS array transducers using piezo-composite materials, and 30 and 35 MHz linear array transducers were designed and fabricated [2-3]. However, most of the applications for HFUS use a single element transducer with different scanning systems for imaging, since the HFUS array system and transducers are much more complicated and expensive. There are several geometrical scanning methods such as a linear scanning method, a sector scanning method, an arc scanning method, a radial scanning method, and a rotational motion of an angled transducer, and so on.

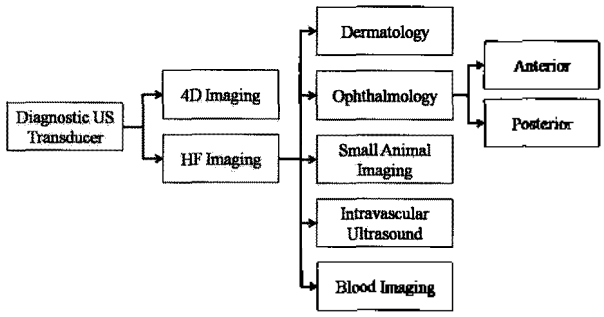

Fig. 1. Summary of the near-future direction of transducer technology. US: ultrasound, 4D: 4-dimension, HF: high frequency.

In this review paper, we summarize the transducer technology for HFUS including the single element transducer with the different scanning methods and the array transducer. Then we review the applications of HFUS to animal and human imaging of vessel and blood.

II. Developments of transducer technology in HFUS

2.1. Single element transducers and mechanical scanning methods

Most of the HFUS systems use a single element transducer and a mechanical scanning system for imaging. Therefore, the single element transducer is the most popular transducer for HFUS applications. The active materials for HFUS transducer are piezoelectric polymers such as poly (vinylidine fluoride) [PVDF] and co-polymer PV (DF-TrFE) [4-5], piezoceramics [6-7], and single crystals such as lithium niobate ($LiNbO_3$) and piezoelectric single crystals based on a relaxor (PZN or PMN) and PT solid solution [8]. Piezoelectric polymers are relatively easy to fabricate since they have a low acoustic impedance (~4 MRayl) and a low dielectric constant ($\varepsilon^S/\varepsilon_0 < 10$), but a poor electromechanical coupling coefficient (k_t <0.3) [7]. It is still used for very high frequency applications or hydrophones. PZT ceramics are mostly often used for the commercial systems, since they have higher electro-mechanical coupling coefficients (k_t = 0.5 for PZT-5H). But they have higher acoustic impedances (~34 MRayl) and very large dielectric constants ($\varepsilon^S/\varepsilon_0$ ~1350). $LiNbO_3$ is ideal for designing sensitive large aperture single element HFUS transducers, displaying good electromechanical coupling (k_t = 0.5), a low

dielectric constant ($\varepsilon^S/\varepsilon_0$< 30), and high longitudinal sound speed (7360 m/s). Though this material has a high acoustic impedance (~34.5 MRayl) and very high electrical and mechanical Q, it was shown to provide improved sensitivity and similar bandwidth when compared to devices from PVDF, lead titanate, and PZT fiber composite [7]. The design and fabrication of the efficient and broadband single element HFUS transducers using $LiNbO_3$ were well summarized in [9].

As for other single crystals such as lead magnesium niobate-lead titanate (PMN-PT), or lead zinc niobate-lead titanate (PZN-PT), they are ideal for small aperture single element HFUS transducer since they have much large dielectric constant ($\varepsilon^S/\varepsilon_0$~797 for PMN-33PT) while they have the similar coupling coefficient (k_t = 0.58) and acoustic impedance (~36.9 MRayl) with $LiNbO_3$. Small aperture (<1.0 mm) PMN-PT transducer was designed and fabricated for 40 MHz [10], and needle-type transducers were also fabricated and applied to measure the flow speed in retinal vessels for a Doppler system [11]. HFUS transducers of 35 MHz and 60 MHz were recently fabricated using lead indium niobate-lead magnesium niobate-lead titanate (0.24 PIN-0.44 PMN-0.32 PT) as an active piezoelectric material. The PIN-PMN-PT single crystal has similar properties (k_t = 0.58, $\varepsilon^S/\varepsilon_0$~700, 32.6 MRayl of acoustic impedance) with PMN-PT, but higher coercivity (6.0 kV/cm) and higher Curie temperature (160 ℃) than PMN-PT crystal (2.5 kV/cm, 131 ℃), leading better thermal stability compared with the PMN-PT transducers [12-13].

There are several scanning methods to get images using a single element transducer. The simplest scanning method is a straight linear motion for a rectangular image format [14-15]. For the concave surface of the eye, an arc scanning method was tried [16]. In IVUS and endoluminal imaging, a radial scanning is popular for a circular imaging format [17]. A cylindrical C-scan method was tried to get an image at a certain depth by combining a straight scanning and a radial scanning [18]. These scanning geometries are shown in Fig. 2 (a) to (d).

High frequency ultrasound over 40 MHz has been used to image the anterior segment of the eye, but it is not suitable for the posterior segment due to the frequency-dependent attenuation of ultrasound and thus the limitation of penetration depth. Therefore, a novel scan method was recently suggested to image the posterior segment of the eye with an angled high frequency US needle transducer as shown in Fig. 2 (e) and (f) [10]. In this method, the needle transducer is inserted into the eye through a small incision hole of 1 mm in diameter and rotated to form a cone-shaped imaging plane, allowing the spatial information of retinal vessels and diagnosis of their occlusion to be displayed. The feasibility of this

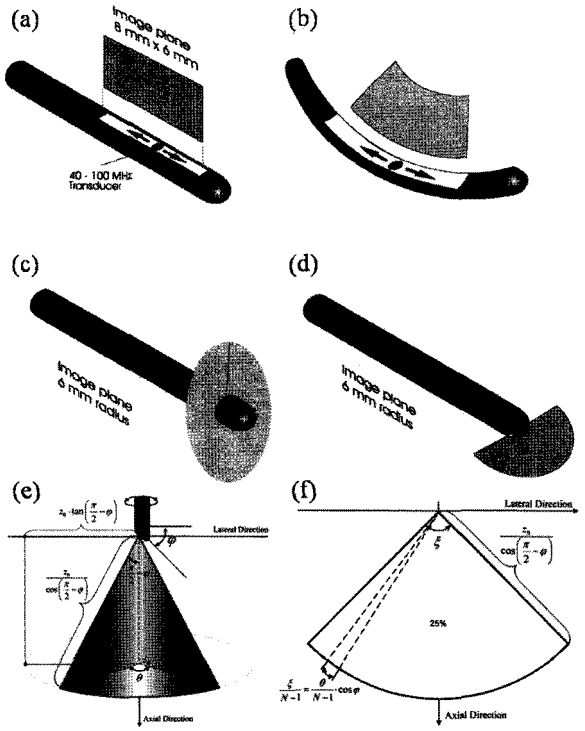

Fig. 2. Scanning geometries for mechanically scanned highfrequency transducers. (a) Linear and (b) arc scanning approaches are used for ocular and skin imaging applications and (c) radial scanning mode is prevalent in intravascular ultrasound and other forms of endoluminal imaging. (d) Look-ahead geometries are still very experimental [69]. Diagram explaining how to convert a 3-D cone-shaped imaging plane (e) into a sector one (f) [10]. When a □-angled needle transducer is partially rotated by an angle of θ, part of a cone is formed (e). The angle of $\pi/2 - \phi$represents half of the opening angle (or aperture) of the cone. If the surface of this partial cone is unfolded, it becomes a sector shape with a central angle of ξ and a radius of $z_0/\cos(\pi/2 - \phi)$ (f).

novel technique was tested with images of a wire phantom, a polyimide tube, and an excised pig eye obtained by manually rotating a 40-MHz PMN-PT needle transducer with a beveled tip of 45°. Rotational scan imaging may help expand the minimally invasive applications of HFUS to other internal tissues where it can be used as a combination with endoscope.

2.2. Linear array transducers

Linear arrays are desired for several reasons, including clinical convenience, increased frame rates, improved and real-time blood flow measurement, and the capability to focus the beam dynamically. Limitations in spatial scale, hardware beamforming, materials, and fabrication methods, however, have precluded the development of operational linear and phased arrays at frequencies over 20 MHz. A method for fabricating fine-scale 2-2 composites suitable for 30-MHz linear array transducers was successfully demonstrated in [19]. High thickness coupling, low mechanical loss, and moderate electrical loss were achieved. The piezo-composite was incorporated into a 30 MHz array that included acoustic matching, an elevation focusing lens, electrical matching, and an air-filled kerf between elements. For higher frequency and more elements, the development of a 64-element 35-MHz composite ultrasonic array was discussed [3]. This array was designed primarily for ocular imaging applications, and features 2-2 composite elements mechanically diced out of a fine-grain high-density Navy Type VI ceramic.

The commercially available array transducer-based ultrasound imaging system that enables micro-ultrasound imaging at center frequencies between 15 and 50 MHz was recently reported [1]. The new scanner uses a laser-machined high-frequency 256 element, linear transducer array capable of forming dynamic diffraction limited beams. The power of the linear array approach is embodied in the uniform high resolution maintained over the full field of view. This leads to greatly expanded scope for real-time functional imaging. The unprecedented images made with the new imaging system will enable many new applications including real-time visualization of flow in the mouse placenta, visualization of flow development in the embryo, studies of embryonic to adult cardiac development/disease, and studies of real-time blood flow in mouse models of tumor angiogenesis.

2.3. Convex array

A single element transducer and a linear array have drawbacks, especially for HFUS applications. The aperture is translated mechanically for a single element transducer, so that it has a fairly low frame rate. For a linear array, its view width may be too narrow to image the whole eye in one imaging plane, and this limitation is more serious for higher frequency due to smaller size of the array transducer. Therefore, convex array transducer was recently proposed to resolve these problems [20]. The images of a dog eye were simulated with the linear array and the convex array. As a result, the convex array gives the wider view area than the linear array. But the fabrication of convex arrays is generally more difficult than linear or phased arrays due to the curvature of the aperture. The radius of curvature and the pitch on the array surface must be accurately maintained in order to minimize the error in beamforming. The ceramic should be fully diced along the elevational direction to prevent cracks. HF convex array transducers were recently designed, fabricated, and tested for a whole view of the eye [21].

III. Animal applications

3.1. Measurement target

The HFUS measurement system should be verified in terms of stability, accuracy and safety applying to animals before the application to human body. High-resolution *in vivo* micro-imaging system (Vevo system) manufactured by VisualSonics Inc. is

the most widely used HFUS measurement system for this kind of animal applications. Vevo 660 system (VisualSonics Inc., Toronto, Canada) was used for early tumor growth in mice bearing melanoma xenografts in a noninvasive longitudinal assay [22].

Mouse models of abdominal aortic aneurysm (AAA) have been commonly used in many laboratories for studying molecular mechanisms of AAA formation and development, as well as for testing novel therapeutic agents in the treatment of AAA. However, because of the small size of the animal, the quantification and characterization of AAA development and progress is difficult, time-consuming and requires the sacrifice of the experimental animals. To solve these problems, Berlex Bioscience group has used the Vevo system [23]. Similarly, the ability of a Vevo 660 was assessed to detect AAAs and sequentially quantify the aortic luminal diameter [24].

A quick noninvasive screen of laboratory animal organ phenotype by high-resolution ultrasound is useful in biomedical research and new drug discovery. During new drug testing, imaging animal at the conscious state avoiding anesthesia does not only speed up the screening process, but also avoids the potential compounding interaction of anesthetic agents with the new drugs. The feasibility of imaging kidney in conscious rats with high-frequency ultrasound was explored by AstraZeneca Pharmaceuticals group [25]. They described the detection of two cases of unilateral congenital hydronephrosis.

Other research group evaluated the possibility to determine intima thickness in the rat carotid artery after balloon injury and to monitor intimal hyperplasia formation by UBM during pharmacological treatment [26]. Similarly, a Catholic University of a Korea research team used a 40 MHz high-frequency ultrasound biomicroscopy (Vevo 770, VisualSonics Inc., Toronto, Canada) to investigate the association between high-echogenic intimal thickening and histologic intimal thickness in the carotid artery. They applied these techniques in rats with normal blood pressure, rats with spontaneous hypertension and rats with atherosclerosis that was induced through a high-lipid diet [27].

For a rat sciatic nerve, Vevo 770 was used to determine whether a new ultrasound imaging device with 30 μm resolution would allow imaging of nerve anatomy and regenerating axons, and whether the data collected from a nerve *in situ* was the same as when the nerve was surgically exposed [28]. As a result, there was a difference in the appearance of the sciatic nerve when viewed through its overlying muscles by Vevo 770. This is because when imaging *in vivo*, a great deal of ultrasound signal is lost before reaching the nerve and thus only the strongest tissue signals are detected.

The macromolecular structure of renal artery ostium was evaluated to better understand the relationship of arterial wall structure to atherogenic susceptibility in this clinically-relevant site of atherosclerosis. Blood velocity profiles were measured at the aortic entrance to the left renal artery of living pigs using a Vevo 2100 system (VisualSonics Inc., Toronto, Canada) equipped with a 30MHz linear transducer [29].

3.2. Measurement technique

HFUS is one of some methods such as magnetic resonance imaging (MRI), electrocardiography (ECG), computed tomography (CT) to measure the biological tissue. And the HFUS method has several advantages such as real time, noninvasive, cost reduced measurement, and so on comparing to other methods. To confirm these advantages and to compare HFUS with MRI, ultrasound scans were performed on the hearts of normal and post myocardial infarction mice with a Vevo770 scanner (VisualSonics, Toronto, Canada) operating at 30 MHz frequency. As a result, ultrasound imaging, followed by 2D image tracking, provides an effective, low cost, mobile method to quantify murine cardiac function accurately and reliably [30].

The pulse-wave velocity has been used as an indicator of vascular stiffness, which can be an early

predictor of cardiovascular mortality. An invasive, easily applicable method for detecting regional pulse wave has been developed and tested to mice [31].

Myocardial elastography is a novel method for noninvasively assessing regional myocardial function, with the advantages of high spatial and temporal resolution and high signal-to-noise ratio (SNR). *in vivo* experiments were performed in anesthetized normal and infarcted mice one day after left anterior descending coronary artery ligation using a high-resolution (30 MHz) ultrasound Vevo 770 system. Results showed that the infarcts underwent thinning rather than thickening during systole [32]. Duchenne muscular dystrophy (mdx) is a severe wasting disease, involving replacement of necrotic muscle tissue by fibrous material and fatty infiltrates. One primary animal model of this human disease is the X chromosome-linked mdx strain of mice. The Vevo system was applied to validate and quantify the capability of both energy and entropy metrics of radio-frequency ultrasonic backscatter to differentiate among normal, dystrophic, and steroid-treated skeletal muscle in the mdx model [33].

Electromechanical wave imaging is a novel technique for the noninvasive mapping of conduction waves in the left ventricle through the combination of electrocardiography gating, high frame rate ultrasound imaging and radio-frequency (RF)-based displacement estimation techniques. And this new technique was developed and described using animal application [34]. HFUS imaging using micro bubble contrast agents is becoming increasingly popular in pre-clinical and small animal studies of anatomy, flow and vascular expression of molecular epitopes [35]. Micro bubbles can be tailored for optimal contrast enhancement in fundamental mode imaging as a result.

IV. Human applications

4.1. Ophthalmology

The first ultrasonic study of ophthalmology was published in 1956 [36]. Ophthalmic ultrasound has been developed into a multifaceted diagnostic discipline, and the basic methods are A-mode and B-mode scan, Doppler techniques and recently developed 3-dimensional approaches. From the mid 1990s, ultrasound biomicroscopy or ultrasound backscatter microscopy (UBM) for the eye has been gradually studied. Vertical cross-section images of a 5 mm diameter area of the central cornea were measured by UBM, and corneal thickness maps were created by computer from corneal thickness data [37]. The technology of ophthalmologic UBM has been developed, so that UBM was capable of imaging the peripheral retina, pars plana, and anterior choroid [38]. In addition, in order to measure the reaction of the eye to the conditioning stimulus, a quantitative method was described for measuring angle recess area and factors associated with appositional angle-closure during dark room provocative testing using UBM [39].

A research team demonstrated specific morphologic patterns in congenital glaucoma after various surgical procedures by means of UBM and to investigate correlations between UBM morphology and the effectiveness of glaucoma surgery in reducing intraocular pressure [40]. The capability of UBM was assessed to describe the early characteristics of the exfoliation syndrome in the zonules of eyes that show no apparent signs of the exfoliation syndrome in the iris or lens [41]. And the usefulness of UBM was demonstrated in detecting the morphological changes in the lens caused by the spontaneous absorption of lens material and to detect fundus abnormalities in a patient with Hallermann-Streiff syndrome [42]. Detecting and following small tumors of the ciliary body is a particular challenge because of their location, but UBM can be successfully applied to measure the tumor and even the growth behavior of the small ciliary body tumors [43-44]. The ciliary sulcus also can be directly measured by UBM [45]. Anterior segment optical coherence tomography was developed for the intraocular measurement, and compared with

UBM [46]. The distribution of UBM parameters was analyzed for the peripheral anterior chamber depth, location of the ciliary body, and iris thickness in the study population and related systemic and ocular factors. As a result, configurations of the anterior ocular segment were quantitatively evaluated [47]. Moreover, iris-sutured foldable posterior chamber intraocular lenses (PCIOLs) could be found using UBM. This provides a unique ability to assess anatomic relationships between structures in the anterior segment of the eye and thus is ideally suited to study iris-sutured PCIOLs [48].

4.2. Dermatology

HFUS is capable of noninvasive, nonionizing and real-time examination of the skin, with a relatively lower cost compared with other procedures such as biopsy and MRI. The use of UBM has attracted the attention of the dermatology community. Particularly, the growing interest in this field can be attributed to the availability of several commercial UBM systems operating in the 20 to 30 MHz frequency range, and to the appearance of several review articles [49-50]. The frequency range was increased for the high resolution and real time measurement of skin imaging [51]. UBM measurements were performed before and after a single exposure to ultraviolet radiation considering ultraviolet effect to skin [52].

Fibrosis is a common late side effect of radiotherapy treatment for cancer patients and is considered to be a dose-limiting factor during the therapy. The skin thickness and the ultrasonic properties of the neck skin with fibrosis in patients were measured and compared with those of control subjects [53]. UBM also can be used to detect changes in skin thickness in a murine model of scleroderma. The application of this technology will provide in-life assessments that allow not only for continued monitoring of the individual animals and reductions in the numbers of animals used, but also for detection of the effects of potential treatments for scleroderma [54]. Using 20-MHz ultrasound assessment, in some case, it was clarified that medium-dose was more effective than low-dose ultraviolet A1 phototherapy for localized scleroderma [55]. For the ultrasonic diagnosis, high variable-frequency US is a recently available technique capable of clearly defining skin layers and deeper structures that provides local perfusion patterns obtained in real time [56]. That means noninvasive US imaging of skin lesions provides clinical information that is highly relevant.

V. Vascular and blood imaging

5.1. Intravascular ultrasound (IVUS)

IVUS is one of the oldest and the most widely used human applications of HFUS. The vascular applications are in the balloon angioplasty, stenting procedures for the treatment of coronary artery disease [57-59], and the assessment of vasculopathy related to heart transplantation [60]. The IVUS applications have been more explored to the areas of combined imaging and interventional tools [61-62], forward looking devices [63], 3-D reconstruction techniques [64-65], improved methods for tissue characterization such as elastography [66-67], and high frequency imaging [68].

In an IVUS system, a catheter with a single element transducer at its tip is rotating in the vessel lumen in order to visualize and measure the vessel wall and any associated plaque form. The aperture size of the IVUS transducer within the catheter whose outer diameters is 0.9 -1.17 mm is limited to the order of 0.5 to 0.75 mm [69]. The fabrication of IVUS catheter is practically difficult so that the high quality of HFUS image is challenging. Because of size limitation, a linear or phased array transducer was difficult to fabricate so the IVUS array transducer was not commercially available yet even though it was developed for the purposes of research [3] [9].

IVUS systems initially started to use 20- to

30-MHz of frequency whose lateral and axial resolutions are of 250-500 μm and 80-100 μm, respectively. In order to provide the images of better resolution of important structures of normal coronary arteries, IVUS systems have been developed to operate at higher frequencies in the 40-50-MHz range [70-72]. However, as frequency increases, the scattering signal from the blood increases rapidly with increasing frequency [69] [73], which causes a problem in defining the boundary between lumen and vessel wall. The increased signal from blood provides an opportunity to develop decorrelation-based color-flow mapping techniques with which to segment the image and estimate volume flow [74] and to investigate the blood properties including red blood cell aggregation [75].

5.2. High-frequency Doppler system

HFUS Doppler in the frequency range over a few tens of MHz can measure blood flow in the microcirculation. Moreover, HFUS Doppler increases sensitivity because the backscattering from blood is increasing with frequency as a 4th power. Therefore, a continuous wave (CW) Doppler ultrasound system with a transducer of a center frequency of 40-MHz using lithium niobate crystals and a 50-MHz pulsed wave (PW) Doppler system with a focused PVDF transducer were developed [76-77]. The CW HFUS Doppler system can detect and measure velocities on the order of the blood velocities found in the capillaries (1 mm/s) and arterioles (5 mm/s) with suitable velocity (50-500 μm/s) and temporal (20-250 ms) resolutions. The PW HFUS system is capable of detecting velocities on the order of the blood velocities found in the capillaries (0.5 mm/s) and arterioles (5 mm/s) with suitable velocity (30-300 μm/s) and temporal (15-100 ms) resolutions with sample volumes with dimensions 70 μm laterally by 90-900 μm axially. *in vivo* measurements demonstrate that PW HF Doppler can detect and measure blood velocities of less than 5 mm/s in arterioles and venules with diameters as small as 20 μm and 35 μm, respectively, using a sample volume of only 70 μm laterally by 150 μm axially [76-77].

Another research group developed high-frequency needle ultrasound transducers with an aperture size of 0.4 mm using PMN-33 % PT as an active piezoelectric material. The measured center frequency and -6 dB fractional bandwidth of the PMN-PT needle transducer were 44 MHz and 45 %, respectively. The two-way insertion loss was approximately 15 dB. *in vivo* high-frequency PW Doppler patterns of blood flow in the posterior portion and in vitro UBM images of the rabbit eye were obtained with the 44-MHz needle transducer [11].

Using the HFUS PW Doppler system, blood flow velocity from choroidal and retinal vessels of rabbits was measured. The average measurement error was 5.97±1.34 %, and the velocities gradually slowed from the disc edge to the distal part, and temporal velocities were faster than nasal velocities at all measurement sites. This study demonstrated the feasibility of reliably measuring retinal blood flow velocity using a 45 MHz ultrasonic Doppler system with a needle transducer [78]. This group also developed the first HF PW Doppler system including a 16-channel HF analog beamformer, a HF PW Doppler module, timing circuits, HF bipolar pulsers and analog front ends using a 30-MHz linear array transducer, assessing the cardiovascular functions in small animals. The two-way beamwidths were determined to be 160 μm to 320 μm when the array was electronically focused at different focal points at depths from 5 to 10 mm. The system is capable of detecting motion velocity of the wire phantom as low as 0.1 mm/s, and detecting blood-mimicking flow velocity in the 127-μm tube lower than 7 mm/s. The system was subsequently used to measure the blood flow *in vivo* in two mouse abdominal superficial vessels, with diameters of approximately 200 μm, and a mouse aorta close to the heart [79].

5.3. Blood echogenicity

Since a red blood cell is a Rayleigh scatterer up to

50 MHz or higher frequency, the backscattering coefficient is a function of the 4th power as shown in Fig. 3. Therefore, as frequency is higher, the backscattering from blood is increasing abruptly while the one from the other tissues increases less. Then the contrast of the backscattered signals between the tissue and blood would be smaller as frequency is higher, leading to potential to see the echo from blood in US images at higher frequency. The sensitivity and resolution are higher at higher frequency, so that HFUS is a good tool to explore the dynamic blood properties *in situ* using B-mode imaging.

Two papers were recently published to measure the pulsatility of echogenicity from whole porcine blood under pulsatile flow using high-frequency [80-81]. In a pulsatile Couette flow apparatus, cyclic variations of the backscattered signals from porcine blood due to changes in shear rate for stroke rates of 20 to 70 beats per minute (BPM) were measured using two single element transducers at 10 and 35 MHz. At 35 MHz, cyclic variations in backscatter were observed from 20 to 70 BPM with its higher magnitude, while they were detected only at 20 BPM at 10 MHz. The increased sensitivity at

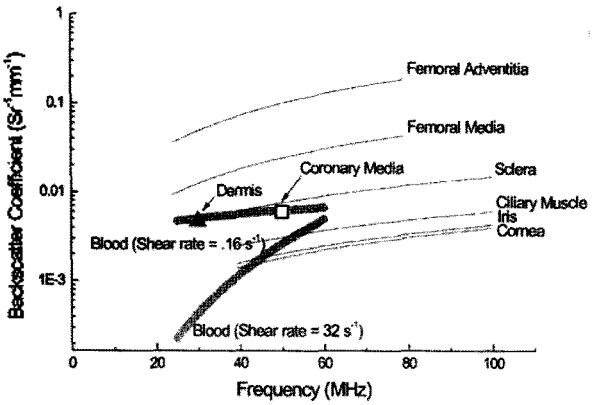

Fig. 3. Ultrasound backscatter coefficients for a variety of tissues in the 20- to 100-MHz range. Solid lines represent extrapolations of measurements for human femoral adventitia and media, human sclera, ciliary muscle, iris, and cornea, and whole human blood at low and high shear rates (wide grey lines). Integrated backscatter coefficients for coronary media and human dermis are also given. All measurements were made at 37℃, with the exception of dermis (22 - 24℃). See original publications for error bars [69].

35 MHz to small changes in aggregate size might be the reason for the better characterization of RBC aggregation at physiological stroke rates, corroborating *in vivo* observations of cyclic blood echogenicity variations in patients using a 30-MHz intravascular ultrasound catheter [80].

In another research [81], the integrated backscatter (IB) and flow velocity as functions of time were calculated directly using RF signals from flowing porcine blood with 3 single-element transducers at frequencies of 10, 35, and 50 MHz in a mock flow loop. Cyclic variations of the IB curve were clearly observed at a low flow velocity and a hematocrit of 40 % when using 50 MHz ultrasound while these cyclic variations were detected only at 10 cm/s when using 10 MHz ultrasound. The peak of the IB curve from whole blood led the peak of the velocity waveform, which could be explained by the assumption that a rapid flow can promote RBC aggregation under pulsatile flow, showing that the sensitivity and resolution of detecting blood properties are higher for 50 MHz ultrasound than for 10 MHz ultrasound.

A superficial cephalic vein in the wrist of a normal subject was examined with a high-frequency (30 MHz) ultrasound system with an annular-array broadband transducer [82]. The echo was enhanced 1 hour after the subject had eaten and was further enhanced when the central side of the vein was compressed. This increased spontaneous echo contrast after a meal appears to resemble the aggregation of erythrocytes and further by compressing larger veins. This intravenous echo contrast in superficial veins may prove useful in the noninvasive study of the physiologic dynamics of erythrocyte aggregation [82].

We also measured the cyclic variation of blood echogenicity from radial artery of a normal subject using a HFUS UBM system of center frequency of 30 MHz [83].

Therefore, HFUS would be a promising tool to explore RBC aggregation *in situ in vivo* noninvasively, which is changed dynamically in time and vessel

position in the near future.

VI. Conclusions

Recent techniques of HFUS and its applications were summarized in animal and human imaging focusing on vascular and blood imaging. HFUS could be applied to the broad areas of the biological tissues and organs even though the penetration depth of ultrasound is small. The HFUS transducer technologies of single element and array transducers were briefly reviewed with applications in small animal imaging for research purposes and in human imaging for ophthalmology and dermatology. Blood imaging and vascular imaging are considered as promising areas of HFUS applications in the near future.

Acknowledgment

This work was supported by the National Research Foundation grant funded by the Korean Government (NRF-2010-0017078).

References

1. F. S. Foster, J. Mehi, M. Lukacs, D. Hirson, C. White, C. Chaggares, and A. Needles, "A New 15-50 MHz Array-Based Micro-Ultrasound Scanner for Preclinical Imaging," *Ultrasound Med. Biol.*, vol. 35, no. 10, pp. 1700-1708, 2009.
2. T. A. Ritter, T. R. Shrout, R. Tutwiler, and K. K. Shung, "A 30-MHz piezo-composite ultrasound array for medical imaging applications," *IEEE Trans. Ultrason. Ferroelectr. Freq. Control*, vol. 49, no. 2, pp. 217-230, 2002.
3. J. M. Cannata, J. A. Williams, Z. Qifa, T. A. Ritter, and K. K. Shung, "Development of a 35-MHz piezo-composite ultrasound array for medical imaging," *IEEE Trans. Ultrason. Ferroelectr. Freq. Control*, vol. 53, no. 1, pp. 224-236, 2006.
4. G. R. Lockwood, D. H. Turnbull, and F. S. Foster, "Fabrication of high frequency spherically shaped ceramic transducers," *IEEE Trans. Ultrason. Ferroelectr. Freq. Control*, vol. 41, no. 2, pp. 231-235, 1994.
5. M. J. Zipparo, K. K. Shung, and T. R. Shrout, "Piezoceramics for high-frequency (20 to 100 MHz) single-element imaging transducers," *IEEE Trans. Ultrason. Ferroelectr. Freq. Control*, vol. 44, no. 5, pp. 1038-1048, 1997.
6. M. D. Sherar and F. S. Foster, "The design and fabrication of high frequency poly(vinylidene fluoride) transducers," *Ultrason. Imaging*, vol. 11, no. 2, pp. 75-94, 1989.
7. K. A. Snook, Z. Jian-Zhong, C. H. F. Alves, J. M. Cannata, C. Wo-Hsing, R. J. Meyer, Jr., T. A. Ritter, and K. K. Shung, "Design, fabrication, and evaluation of high frequency, single-element transducers incorporating different materials," *IEEE Trans. Ultrason. Ferroelectr. Freq. Control*, vol. 49, no. 2, pp. 169-176, 2002.
8. D. A. Knapik, B. Starkoski, C. J. Pavlin, and F. S. Foster, "A 100-200 MHz ultrasound biomicroscope," *IEEE Trans. Ultrason. Ferroelectr. Freq. Control*, vol. 47, no. 6, pp. 1540-1549, 2000.
9. J. M. Cannata, T. A. Ritter, C. Wo-Hsing, R. H. Silverman, and K. K. Shung, "Design of efficient, broadband single-element (20-80 MHz) ultrasonic transducers for medical imaging applications," *IEEE Trans. Ultrason. Ferroelectr. Freq. Control*, vol. 50, no. 11, pp. 1548-1557, 2003.
10. D.-G. Paeng, J. H. Chang, R. Chen, M. S. Humayun, and K. K. Shung, "Feasibility of rotational scan ultrasound imaging by an angled high frequency transducer for the posterior segment of the eye," *IEEE Trans. Ultrason. Ferroelectr. Freq. Control*, vol. 56, no. 3, pp. 676-680, 2009.
11. Q. Zhou, X. Xu, E. L. Gottlieb, S. Lei, J. M. Cannata, H. Ameri, M. S. Humayun, H. Pengdi, and S. K. Shung, "PMN-PT single crystal, high-frequency ultrasonic needle transducers for pulsed-wave Doppler application," *IEEE Trans. Ultrason. Ferroelectr. Freq. Control*, vol. 54, no. 3, pp. 668-675, 2007.
12. X. Xu, Q. Zhou, H. Ameri, E. J. Gottlieb, B. Lai, J. T. Yen, J. M. Cannata, H. Pengdi, M. S. Humayun, and K. K. Shung, "High-Frequency Pulsed-Wave Ultrasound Doppler System for Biomedical Applications with PMN-PT Needle Transducer and 30 MHz Linear Array," *Ultrasonics Symposium, 2006. IEEE*, 2006.
13. S. Ping, Z. Qifa, Z. Benpeng, W. Dawei, H. Changhong, J. M. Cannata, T. Jin, H. Pengdi, W. Gaoleng, and K. K. Shung, "Design and fabrication of PIN-PMN-PT single-crystal high-frequency ultrasound transducers," *IEEE Trans. Ultrason. Ferroelectr. Freq. Control*, vol. 56, no. 12, pp. 2760-2763, 2009.
14. F. S. Foster, G. R. Lockwood, L. K. Ryan, K. A. Harasiewicz, L. Berube, and A. M. Rauth, "Principles and applications of ultrasound backscatter microscopy," *IEEE Trans. Ultrason. Ferroelectr. Freq. Control*, vol. 40, no. 5, pp. 608-617, 1993.
15. G. R. Lockwood, D. H. Turnball, D. A. Christopher, and F. S. Foster, "Beyond 30 MHz [applications of high-frequency ultrasound imaging]," *IEEE Eng. Med. Biol. Mag.*, vol. 15, no. 6, pp. 60-71, 1996.
16. R. H. Silverman, D. Z. Reinstein, T. Raevsky, and D. J. Coleman, "Improved system for sonographic imaging and biometry of the cornea," *J. Ultrasound Med.*, vol. 16, no. 2, pp. 117-124, 1997.
17. M. Eberle, "The latest in electronic imaging," *Seminars in interventional cardiology*, vol. 2, no., pp. 19-23, 1997.
18. K. Yokosawa, R. Shinomura, S. Sano, Y. Ito, S. Ishikawa, and Y. Sato, "A 120-MHz Ultrasound Probe for Tissue Imaging," *Ultrason. Imaging*, vol. 18, no. 4, pp. 231-239, 1996.
19. T. A. Ritter, T. R. Shrout, R. Tutwiler, and K. K. Shung, "A 30-MHz piezo-composite ultrasound array for medical imaging applications," *IEEE Trans. Ultrason. Ferroelectr. Freq. Control*, vol. 49, no. 2, pp. 217-230, 2002.
20. H. H. Kim, J. H. Chang, J. M. Cannata, and K. K. Shung, "Design of 20 MHz Convex Array Transducers for High Frequency Ophthalmic Imaging," *Ultrasonics Symposium, 2007. IEEE*, 2007.

21. H. H. Kim, J. M. Cannata, J. A. Williams, J. H. Chang, and K. K. Shung, "Fabrication of 20 MHz convex array transducers for high frequency ophthalmic imaging," *Ultrasonics Symposium (IUS), 2009 IEEE International*, 2009.
22. A. M. Y. Cheung, A. S. Brown, L. A. Hastie, V. Cucevic, M. Roy, J. C. Lacefield, A. Fenster, and F. S. Foster, "Three-dimensional ultrasound biomicroscopy for xenograft growth analysis," *Ultrasound Med. Biol.*, vol. 31, no. 6, pp. 865-870, 2005.
23. B. Martin-McNulty, J. Vincelette, R. Vergona, M. E. Sullivan, and Y.-X. Wang, "Noninvasive measurement of abdominal aortic aneurysms in intact mice by a high-frequency ultrasound imaging system," *Ultrasound Med. Biol.*, vol. 31, no. 6, pp. 745-749, 2005.
24. C. Barisione, R. Charnigo, D. A. Howatt, J. J. Moorleghen, D. L. Rateri, and A. Daugherty, "Rapid dilation of the abdominal aorta during infusion of angiotensin II detected by noninvasive high-frequency ultrasonography," *J. Vasc. Surg.*, vol. 44, no. 2, pp. 372-376, 2006.
25. Y.-X. J. Wang, G. Betton, E. Floettmann, E. Fantham, and G. Ridgwell, "Imaging Kidney in Conscious Rats with High-Frequency Ultrasound and Detection of Two Cases of Unilateral Congenital Hydronephrosis," *Ultrasound Med. Biol.*, vol. 33, no. 3, pp. 483-486, 2007.
26. A. Razuvaev, K. Lund, J. Roy, U. Hedin, and K. Caidahl, "Noninvasive real-time imaging of intima thickness after rat carotid artery balloon injury using ultrasound biomicroscopy," *Atherosclerosis*, vol. 199, no. 2, pp. 310-316, 2008.
27. Y.-S. Choi, H.-J. Youn, J.-S. Youn, C.-S. Park, Y.-S. Oh, and W.-S. Chung, "Measurement of the Intimal Thickness of the Carotid Artery: Comparison Between 40 MHz Ultrasound and Histology in Rats," *Ultrasound Med. Biol.*, vol. 35, no. 6, pp. 962-966, 2009.
28. D. P. Kuffler, "Ultrasound imaging of regenerating rat sciatic nerves in situ," *Journal of Neuroscience Methods*, vol. 188, no. 2, pp. 276-279, 2010.
29. E. B. Neufeld, Z.-X. Yu, D. Springer, Q. Yu, and R. S. Balaban, "The renal artery ostium flow diverter: Structure and potential role in *atherosclerosis*," Atherosclerosis, vol. In Press, Corrected Proof, no. 2010.
30. Y. Li, C. D. Garson, Y. Xu, R. J. Beyers, F. H. Epstein, B. A. French, and J. A. Hossack, "Quantification and MRI Validation of Regional Contractile Dysfunction in Mice Post Myocardial Infarction Using High Resolution Ultrasound," *Ultrasound Med. Biol.*, vol. 33, no. 6, pp. 894-904, 2007.
31. K. Fujikura, J. Luo, V. Gamarnik, M. Pernot, R. Fukumoto, M. D. Tilson, and E. E. Konofagou, "A Novel Noninvasive Technique for Pulse-Wave Imaging and Characterization of Clinically-Significant Vascular Mechanical Properties In Vivo," *Ultrason. Imaging*, vol. 29, no., pp. 137-154, 2007.
32. J. Luo, K. Fujikura, S. Homma, and E. E. Konofagou, "Myocardial Elastography at Both High Temporal and Spatial Resolution for the Detection of Infarcts," *Ultrasound Med. Biol.*, vol. 33, no. 8, pp. 1206-1223, 2007.
33. K. D. Wallace, J. N. Marsh, S. L. Baldwin, A. M. Connolly, R. Keeling, G. M. Lanza, S. A. Wickline, and M. S. Hughes, "Sensitive Ultrasonic Delineation of Steroid Treatment in Living Dystrophic Mice with Energy-Based and Entropy-Based Radio Frequency Signal Processing," *IEEE Trans. Ultrason. Ferroelectr. Freq. Control*, vol. 54, no. 11, pp. 2291-2299, 2007.
34. E. E. Konofagou, J. Luo, D. Saluja, D. O. Cervantes, J. Coromilas, and K. Fujikura, "Noninvasive electromechanical wave imaging and conduction-relevant velocity estimation in vivo," *Ultrasonics*, vol. 50, no. 2, pp. 208-215, 2010.
35. S. Sirsi, J. Feshitan, J. Kwan, S. Homma, and M. Borden, "Effect of Microbubble Size On Fundamental Mode High Frequency Ultrasound Imaging In Mice," *Ultrasound Med. Biol.*, vol. In Press, Corrected Proof, no. 2010.
36. G. H. Mundt and W. F. Hughes, "Ultrasonics in ocular diagnosis," *Am. J. Ophthalmol.*, vol. 42, no., pp. 488-498, 1956.
37. I. Wada, "Ultrasound biomicroscopic corneal thickness measurement for corneal thickness mapping," *Jpn. J. Ophthalmol.*, vol. 41, no. 1 pp. 12-18, 1996.
38. R. C. Gentile, D. M. Berinstein, J. Liebmann, R. Rosen, Z. Stegman, C. Tello, J. B. Walsh, and R. Ritch, "High-resolution ultrasound biomicroscopy of the pars plana and peripheral retina. Historical vignette," *Ophthalmology*, vol. 105, no. 3, pp. 478-484, 1998.
39. H. Ishikawa, K. Esaki, J. M. Liebmann, Y. Uji, and R. Ritch, "Ultrasound Biomicroscopy Dark Room Provocative Testing: A Quantitative Method for Estimating Anterior Chamber Angle Width," *Jpn. J. Ophthalmol.*, vol. 43, no. 6, pp. 526-534, 1999.
40. T. S. Dietlein, B. F. Engels, P. C. Jacobi, and G. K. Krieglstein, "Ultrasound biomicroscopic patterns after glaucoma surgery in congenital glaucoma," *Ophthalmology*, vol. 107, no. 6, pp. 1200-1205, 2000.
41. K. Inazumi, D. Takahashi, T. Taniguchi, and T. Yamamoto, "Ultrasound Biomicroscopic Classification of Zonules in Exfoliation Syndrome," *Jpn. J. Ophthalmol.*, vol. 46, no. 5, pp. 502-509, 2002.
42. M. Sato, H. Terasaki, E. Amano, Y. Okamoto, and Y. Miyake, "Ultrasound Biomicroscopic Findings in Hallerman-Streiff Syndrome," *Jpn. J. Ophthalmol.*, vol. 46, no. 4, pp. 451-454, 2002.
43. D. J. Weisbrod, C. J. Pavlin, K. Emara, M. A. Mandell, J. McWhae, and E. R. Simpson, "Small Ciliary Body Tumors: Ultrasound Biomicroscopic Assessment and Follow-up of 42 Patients," *Am. J. Ophthalmol.*, vol. 141, no. 4, pp. 622-628, 2006.
44. D. J. Weisbrod, C. J. Pavlin, W. Xu, and E. R. Simpson, "Long-term Follow-up of 42 Patients with Small Ciliary Body Tumors with Ultrasound Biomicroscopy," *Am. J. Ophthalmol.*, vol. 149, no. 4, pp. 616-622, 2010.
45. J. Oh, H.-H. Shin, J.-H. Kim, H.-M. Kim, and J.-S. Song, "Direct Measurement of the Ciliary Sulcus Diameter by 35-Megahertz Ultrasound Biomicroscopy," *Ophthalmology*, vol. 114, no. 9, pp. 1685-1688, 2007.
46. C. J. Pavlin, L. M. V squez, R. Lee, E. R. Simpson, and I. I. K. Ahmed, "Anterior Segment Optical Coherence Tomography and Ultrasound Biomicroscopy in the Imaging of Anterior Segment Tumors," *Am. J. Ophthalmol.*, vol. 147, no. 2, pp. 214-219.e2, 2009.
47. I. M. Henzan, A. Tomidokoro, C. Uejo, H. Sakai, S. Sawaguchi, A. Iwase, and M. Araie, "Ultrasound Biomicroscopic Configurations of the Anterior Ocular Segment in a Population-Based Study: The Kumejima Study," *Ophthalmology*, vol. In Press, Corrected Proof, no. 2010.
48. J. J. Mura, C. J. Pavlin, G. P. Condon, G. W. Belovay, C. F. Kranemann, H. Ishikawa, and I. I. K. Ahmed, "Ultrasound Biomicroscopic Analysis of Iris-Sutured Foldable Posterior Chamber Intraocular Lenses," *Am. J. Ophthalmol.*, vol. 149, no. 2, pp. 245-252.e2, 2010.
49. D. A. Perednia, "What dermatologists should know about digital imaging," *Journal of the American Academy of Dermatology*, vol.

25, no. 1, Part 1, pp. 89-108, 1991.
50. C. A. Gropper, M. J. Stiller, J. L. Shupack, J. Driller, M. Rorke, and F. Lizzi, "Diagnostic high resolution ultrasound in dermatology," *Int. J. Dermatol.*, vol. 32, no., pp. 243-250, 1993.
51. D. H. Turnbull, B. G. Starkoski, K. A. Harasiewicz, J. L. Semple, L. From, A. K. Gupta, D. N. Sauder, and F. S. Foster, "A 40-100 MHz B-scan ultrasound backscatter microscope for skin imaging," *Ultrasound Med. Biol.*, vol. 21, no. 1, pp. 79-88, 1995.
52. H. Lopez, J. Z. Beer, S. A. Miller, and B. Z. Zmudzka, "Ultrasound measurements of skin thickness after UV exposure: a feasibility study," *Journal of Photochemistry and Photobiology B: Biology*, vol. 73, no. 3, pp. 123-132, 2004.
53. Y. P. Huang, Y. P. Zheng, S. F. Leung, and A. P. C. Choi, "High Frequency Ultrasound Assessment of Skin Fibrosis: Clinical Results," *Ultrasound Med. Biol.*, vol. 33, no. 8, pp. 1191-1198, 2007.
54. J. L. Tedstone, S. M. Richards, R. D. Garman, and M. C. Ruzek, "Ultrasound Imaging Accurately Detects Skin Thickening in a Mouse Scleroderma Model," *Ultrasound Med. Biol.*, vol. 34, no. 8, pp. 1239-1247, 2008.
55. P.-G. Salor, S. Radakovic, K. Schulmeister, H. H nigsmann, and A. Tanew, "Medium-dose is more effective than low-dose ultraviolet A1 phototherapy for localized scleroderma as shown by 20-MHz ultrasound assessment," *Journal of the American Academy of Dermatology*, vol. 60, no. 5, pp. 786-791, 2009.
56. X. Wortsman and J. Wortsman, "Clinical usefulness of variable-frequency ultrasound in localized lesions of the skin," *Journal of the American Academy of Dermatology*, vol. 62, no. 2, pp. 247-256, 2010.
57. S. Goldberg, A. Colombo, S. Nakamura, Y. Almagor, L. Maiello, and J. Tobis, "Benefit of intracoronary ultrasound in the deployment of Palmaz-Schatz stents," *J Am Coll Cardiol*, vol. 24, no. 4, pp. 996-1003, 1994.
58. A. Colombo, P. Hall, S. Nakamura, Y. Almagor, L. Maiello, G. Martini, A. Gaglione, S. L. Goldberg, and J. M. Tobis, "Intracoronary Stenting Without Anticoagulation Accomplished With Intravascular Ultrasound Guidance," *Circulation*, vol. 91, no. 6, pp. 1676-1688, 1995.
59. I. Moussa, C. Di Mario, L. Di Francesco, B. Reimers, S. Blengino, and A. Colombo, "Subacute Stent Thrombosis and the Anticoagulation Controversy: Changes in Drug Therapy, Operator Technique, and the Impact of Intravascular Ultrasound," *The American Journal of Cardiology*, vol. 78, no. 3, Supplement 1, pp. 13-17, 1996.
60. V. Klauss, J. Rieber, P. Uberfuhr, K. Theisen, and H. Mudra, "Qualitative and quantitative assessment of cardiac allograft vasculopathy by intravascular ultrasound," *Transplantation Proceedings*, vol. 2, no., pp. 1975-1976, 1995.
61. P. J. Fitzgerald, M. Belef, A. J. Connolly, K. Sudhir, and P. G. Yock, "Design and initial testing of an ultrasound-guided directional atherectomy device," *American heart journal*, vol. 129, no. 3, pp. 593-598, 1995.
62. M. Kawata, T. Okada, N. Igarashi, K. Okajima, Y. Domoto, and T. Mizutani, "Assessment of intravascular ultrasound-bearing balloon catheter-guided percutaneous transluminal coronary angioplasty and stenting," *Heart and Veseels*, vol. Suppl 12, no., pp. 185-187, 1997.
63. D. Liang and B. Hu, "Forward-looking catheters," *Seminars in Interventional Cardiology*, vol. 2, no. 1, pp. 75-87, 1997.
64. C. von Birgelen, R. Erbel, C. Di Mario, W. Li, F. Prati, J. Ge, N. Bruining, G. G rge, C. Slager, P. Serruys, and e. al., "Three-dimensional reconstruction of coronary arteries with intravascular ultrasound," *Herz*, vol. 20, no. 4, pp. 277-289, 1995.
65. C. von Birgelen, W. Li, N. Bom, and P. Serruys, "Quantitative three-dimensional intravascular ultrasound," *Seminars in interventional cardiology*, vol. 2, no. 1, pp. 25-32, 1997.
66. E. Cespedes, C. de Korte, A. van der Steen, C. von Birgelen, and C. Lancee, "Intravascular elastography: principles and potentials," *Seminars in interventional cardiology* vol. 2, no., pp. 55-62, 1997.
67. C. L. de Korte, A. F. W. van der Steen, E. I. C spedes, and G. Pasterkamp, "Intravascular Ultrasound Elastography in Human Arteries: Initial Experience In Vitro," *Ultrasound Med. Biol.*, vol. 24, no. 3, pp. 401-408, 1998.
68. F. Foster, D. Knapik, J. Machado, J. Gallet, L. Ryan, and S. Nissen, "High frequency intracoronary ultrasound imaging," *Seminars in interventional cardiology*, vol. 2, no., pp. 33-41, 1997.
69. F. S. Foster, C. J. Pavlin, K. A. Harasiewicz, D. A. Christopher, and D. H. Turnbull, "Advances in ultrasound biomicroscopy," *Ultrasound Med. Biol.*, vol. 26, no. 1, pp. 1-27, 2000.
70. C. Di Mario, S. The, S. Madretsma, R. van Suylen, R. Wilson, N. Bom, P. Serruys, E. Gussenhoven, and R. JR, "Detection and characterization of vascular lesions by intravascular ultrasound: an in vitro study correlated with histology," *Journal of the American Society of Echocardiography*, vol. 5, no. 2, pp. 135-146, 1992.
71. G. Lockwood, L. Ryan, A. Gotlieb, E. Lonn, J. Hunt, P. Liu, and F. Foster, "In vitro high resolution intravascular imaging in muscular and elastic arteries," *J Am Coll Cardiol*, vol. 20, no. 1, pp. 153-160, 1992.
72. A. J. Martin, L. K. Ryan, A. I. Gollieb, R. M. Henkelman, and F. S. Foster, "Arterial imaging: comparison of high-resolution US and MR imaging with histologic correlation," *Radiographics*, vol. 17, no. 1, pp. 189-202, 1997.
73. F. S. Foster, H. Obara, T. Bloomfield, L. K. Ryan, and G. R. Lockwood, "Ultrasound backscatter from blood in the 30 to 70 MHz frequency range," *Ultrasonics Symposium, 1994. Proceedings., 1994 IEEE*, 1994.
74. W. Li, C. Lancee, A. van der Steen, E. Gussenhoven, and N. Bom, "Blood velocity estimation with high frequency intravascular ultrasound," *Ultrasonics Symposium, 1996. Proceedings., 1996 IEEE*, 1996.
75. S.-H. Wang and K. K. Shung, "In vivo measurements of ultrasonic backscattering in blood," *IEEE Trans. Ultrason. Ferroelectr. Freq. Control*, vol. 48, no. 2, pp. 425-431, 2001.
76. D. A. Christopher, P. N. Burns, J. Armstrong, and F. S. Foster, "A high-frequency continuous-wave Doppler ultrasound system for the detection of blood flow in the microcirculation," *Ultrasound Med. Biol.*, vol. 22, no. 9, pp. 1191-1203, 1996.
77. D. A. Christopher, P. N. Burns, B. G. Starkoski, and F. S. Foster, "A high-frequency pulsed-wave Doppler ultrasound system for the detection and imaging of blood flow in the microcirculation," *Ultrasound Med. Biol.*, vol. 23, no. 7, pp. 997-1015, 1997.
78. N. Matsuoka, D.-G. Paeng, R. Chen, H. Ameri, W. Abdallah, Q. Zhou, A. Fawzi, K. Shung, and M. Humayun, "Ultrasonic Doppler measurements of blood flow velocity of rabbit retinal vessels using a 45-MHz needle transducer," *Graefe's Archive for Clinical and Experimental Ophthalmology*, vol. 248, no. 5, pp. 675-680, 2010.
79. X. Xu, L. Sun, J. M. Cannata, J. T. Yen, and K. K. Shung, "High-Frequency Ultrasound Doppler System for Biomedical

Applications with a 30-MHz Linear Array," *Ultrasound Med. Biol.*, vol. 34, no. 4, pp. 638-646, 2008.
80. L. C. Nguyen, F. T. H. Yu, and G. Cloutier, "Cyclic Changes in Blood Echogenicity Under Pulsatile Flow Are Frequency Dependent," *Ultrasound Med. Biol.*, vol. 34, no. 4, pp. 664-673, 2008.
81. C.-C. Huang, "Cyclic Variations of High-Frequency Ultrasonic Backscattering From Blood Under Pulsatile Flow," *IEEE Trans. Ultrason. Ferroelectr. Freq. Control*, vol. 56, no. 8, pp. 1677-1688, 2009.
82. Y. Sugata and K. Nemoto, "Intravascular Spontaneous Echo Contrast in Superficial Veins: Enhancement by Compression of the Central Side of the Vein and Intake of Food," *Journal of Medical Ultrasonics*, vol. 31, no. 3, pp. J179-J182, 2004.
83. T.-H. Bok, Y. Li, D.-G. Paeng, and H.-J. Kang, "Observation of the cyclic variation of echogenicity in the radial artery using ultrasound biomicroscopy," *Acoustical Society of Korea Conference*, 2010.

[Profile]

• **Tae-Hoon Bok**

1997. 3 ~ 2004. 2: B.S., Dept. of Earth and Marine Science, Hanyang University
2004. 3 ~ 2006. 2: M.S., Dept. of Earth and Marine Science, Hanyang University
2006. 3 ~ present: Ph. D. course, Dept. of Ocean System Engineering, Jeju National University

• **Dong-Guk Paeng**

The Journal of the Acoustical Society of Korea, vol. 24, no. 4E, 2005.